

## C–H Activation

C–H Bond Activation by Early Transition Metal Carbide Cluster Anion  $\text{MoC}_3^-$ Zi-Yu Li,<sup>[a]</sup> Lianrui Hu,<sup>[b]</sup> Qing-Yu Liu,<sup>[a]</sup> Chuan-Gang Ning,<sup>[c]</sup> Hui Chen,<sup>\*,[b]</sup> Sheng-Gui He,<sup>\*,[a]</sup> and Jiannian Yao<sup>[a, b]</sup>

**Abstract:** Although early transition metal (ETM) carbides can activate C–H bonds in condensed-phase systems, the electronic-level mechanism is unclear. Atomic clusters are ideal model systems for understanding the mechanisms of bond activation. For the first time, C–H activation of a simple alkane (ethane) by an ETM carbide cluster anion ( $\text{MoC}_3^-$ ) under thermal-collision conditions has been identified by using high-resolution mass spectrometry, photoelectron imaging spectroscopy, and high-level quantum chemical calculations. Dehydrogenation and ethene elimination were ob-

served in the reaction of  $\text{MoC}_3^-$  with  $\text{C}_2\text{H}_6$ . The C–H activation follows a mechanism of oxidative addition that is much more favorable in the carbon-stabilized low-spin ground electronic state than in the high-spin excited state. The reaction efficiency between the  $\text{MoC}_3^-$  anion and  $\text{C}_2\text{H}_6$  is low ( $0.23 \pm 0.05$ )%. A comparison between the anionic and a highly efficient cationic reaction system ( $\text{Pt}^+ + \text{C}_2\text{H}_6$ ) was made. It turned out that the potential-energy surfaces for the entrance channels of the anionic and cationic reaction systems can be very different.

## Introduction

C–H activation of alkanes, the major constituents of natural gas and oil, is the crucial step for direct transformation of saturated hydrocarbons into value-added products and is a challenging task in chemistry.<sup>[1]</sup> Transition metals and their complexes have been widely studied for C–H activation. The most common mechanism of C–H activation by the metal centers is oxidative addition, by which a C–H bond is cleaved and M–C and M–H bonds are formed.<sup>[1c,2]</sup> For oxidative addition of C–H bonds, the late transition metals, mostly the platinum-group metals Pt, Ir, Os, Ru, Rh, and Pd, have been extensively reported to be reactive, whereas reactive early transition metals (ETMs) were much less reported in condensed-phase studies.<sup>[1c,2–3]</sup>

In contrast to the condensed phase, many gas-phase atomic ions of ETMs can activate C–H bonds of small alkane molecules through oxidative addition under thermal-collision conditions. Examples are the reactions of  $\text{Sc}^+$ ,<sup>[4]</sup>  $\text{Ti}^+$ ,<sup>[5]</sup>  $\text{V}^+$ ,<sup>[6]</sup>  $\text{Y}^+$ ,<sup>[4]</sup>  $\text{Zr}^+$ ,<sup>[7]</sup>  $\text{Nb}^+$ ,<sup>[8]</sup>  $\text{La}^+$ ,<sup>[4]</sup>  $\text{Lu}^+$ ,<sup>[4]</sup>  $\text{Ta}^+$ ,<sup>[9]</sup> and  $\text{W}^+$ <sup>[10]</sup> with ethane. In these reactions, the atomic ions usually have high-spin ground electronic states (exceptions are  $\text{Y}^+$  and  $\text{Lu}^+$  with  $^1\text{S}$  ground states) that are intrinsically unfavorable for oxidative addition.<sup>[11]</sup> The observed reactivity is mostly due to spin crossover from reactive low-spin excited states.<sup>[12]</sup> An example of the importance of low-spin states in oxidative addition is the thermal dehydrogenation reaction of  $\text{CH}_4$  with  $\text{Cr}^+$ : the high-spin ground and excited states ( $^6\text{S}$  and  $^6\text{D}$ ) of  $\text{Cr}^+$  are inert, whereas the low-spin excited states ( $^4\text{D}$  and possibly  $^4\text{G}$ ) of this ion are very reactive.<sup>[11b]</sup> Investigations of late transition metal ions ( $\text{Fe}^+$ ,  $\text{Co}^+$ ,  $\text{Ni}^+$ ,  $\text{Ru}^+$ ,  $\text{Rh}^+$ ,  $\text{Os}^+$ ,  $\text{Ir}^+$ ,  $\text{Pt}^+$ , and  $\text{Au}^+$ )<sup>[12c,13]</sup> in oxidative addition of C–H bonds have also emphasized the importance of low-spin states. For example, the C–H activation of propane by  $\text{Fe}^+$  occurs after spin conversion from the ground-state  $\text{Fe}^+$  ( $^6\text{D}$ ,  $4s^13d^6$ ) $\text{C}_3\text{H}_8$  surface to the low-lying first excited-state  $\text{Fe}^+$  ( $^4\text{F}$ ,  $3d^7$ ) $\text{C}_3\text{H}_8$  surface.<sup>[13a]</sup>

Besides atomic ions, gas-phase atomic clusters, which are generally considered to be ideal models for active sites of condensed-phase systems,<sup>[1d–f,14,15]</sup> have also been investigated for C–H activation. In line with the findings of condensed-phase studies, many atomic clusters of noble metals including  $\text{Pt}$ ,<sup>[16]</sup>  $\text{Pd}$ ,<sup>[17]</sup>  $\text{Rh}$ ,<sup>[18]</sup> their alloys,<sup>[19]</sup> and ligated systems<sup>[20]</sup> are reactive with simple alkane molecules under thermal-collision conditions. However, studied atomic clusters of ETMs such as  $\text{Nb}_n^+$ ,<sup>[21]</sup>  $\text{Nb}_n$ , and  $\text{Ta}_n$  ( $n > 2$ )<sup>[22]</sup> are inert or much less reactive than the atomic species ( $\text{Nb}^+$  and  $\text{Ta}^+$ )<sup>[8,9,12a,b]</sup> in the reaction with simple alkanes. It is important to investigate how to engineer

[a] Z.-Y. Li, Q.-Y. Liu, Prof. Dr. S.-G. He, Prof. Dr. J. Yao  
Beijing National Laboratory for Molecular Science  
State Key Laboratory for Structural Chemistry  
of Unstable and Stable Species, Institute of Chemistry  
Chinese Academy of Sciences, Beijing 100190 (P. R. China)  
E-mail: shengguihe@iccas.ac.cn

[b] L. Hu, Prof. Dr. H. Chen, Prof. Dr. J. Yao  
Beijing National Laboratory for Molecular Sciences  
Key Laboratory of Photochemistry  
Institute of Chemistry, Chinese Academy of Sciences  
Beijing 100190 (P. R. China)  
E-mail: chen@iccas.ac.cn

[c] Prof. Dr. C.-G. Ning  
Department of Physics  
State Key Laboratory of Low-Dimensional Quantum Physics  
Tsinghua University, Beijing 100084 (P. R. China)

Supporting information for this article is available on the WWW under <http://dx.doi.org/10.1002/chem.201503060>.

ETM centers (e.g., by introducing main group elements)<sup>[12c,23]</sup> to form cluster species to activate C–H bonds. ETM oxide clusters have been extensively studied for C–H activation, but it turned out that most of the active centers are oxygen radicals rather than the metal atoms.<sup>[1f,24]</sup>

Herein, we report that carbide clusters of ETMs such as molybdenum can be an important type of species to activate C–H bonds through oxidative addition. It is known that supported molybdenum carbide nanoparticles can be active catalysts for dehydroaromatization of methane to benzene,<sup>[25]</sup> dehydrogenation of ethane and propane to olefins,<sup>[26]</sup> and other reactions in condensed-phase systems. Studies on the reactions between molybdenum carbide clusters and alkane molecules serve as an important approach to discover the mechanism of C–H activation by related carbides at the strictly molecular level. It is noteworthy that the structures and stabilities of the gas-phase ETM carbide clusters have been extensively studied,<sup>[27]</sup> whereas their reactivity has rarely been reported.<sup>[28]</sup>

In this work, high-resolution mass spectrometry, anion photoelectron imaging (PEI) spectroscopy, and high-level quantum chemical calculations were employed to show that thermal ethane conversion to ethene and hydrogen can be facilitated by molybdenum carbide cluster anion  $\text{MoC}_3^-$ . This result is in contrast to the fact that the atomic species  $\text{Mo}^+$ ,  $\text{Mo}^-$ , and  $\text{Mo}$  are all inert toward alkanes under thermal-collision conditions.<sup>[11c,29]</sup> The observed reactivity of  $\text{MoC}_3^-$  thus emphasizes the importance of carburization in engineering the molybdenum center for C–H activation. Anionic clusters were generally found to be much less reactive than their cationic counterparts in reactions with alkane molecules.<sup>[1f,29a,30]</sup> Hence, C–H activation by cluster anions has been much less investigated. However, the reactivity of cluster anions can be interpreted on the basis of reliable electronic structures that can be probed by the powerful anion photoelectron spectroscopy.<sup>[31]</sup> The cluster reaction mechanism can then be compared with those of studied atomic ions ( $\text{M}^+$ ) with well-known electronic structures.

## Results

### Reactivity

The  $\text{MoC}_3^-$  cluster anions were generated by laser ablation, mass-selected, and then introduced into an ion-trap reactor,<sup>[32]</sup> where they were thermalized through collisions with 8–10 Pa He for about 1.5 ms ( $\approx 2400$  collisions) and then interacted with  $\text{C}_2\text{H}_6$ ,  $\text{C}_2\text{D}_6$ , or  $\text{CH}_3\text{CD}_3$  for a period of time (see Experimental Section for more information including ion thermalization). As shown in Figure 1 a,  $\text{MoC}_3^-$  can react with a trace amount of  $\text{H}_2\text{O}$  impurity in the gas-handling system to generate  $\text{MoC}_3\text{O}^-$  ( $\text{MoC}_3^- + \text{H}_2\text{O} \rightarrow \text{MoC}_3\text{O}^- + \text{H}_2$ ), which indicates that  $\text{MoC}_3^-$  is very reductive. On interaction with 0.23 Pa  $\text{C}_2\text{H}_6$  in the reactor for about 6.4 ms, two products peaks assigned to  $\text{MoC}_5\text{H}_4^-$  and  $\text{MoC}_3\text{H}_2^-$  were generated (Figure 1 b). The relative intensities of these products increase with increasing  $\text{C}_2\text{H}_6$  pressure (Figure 1 c), which suggests the dehydrogenation and ethene-elimination reaction channels shown as Equations (1) and (2), respectively.

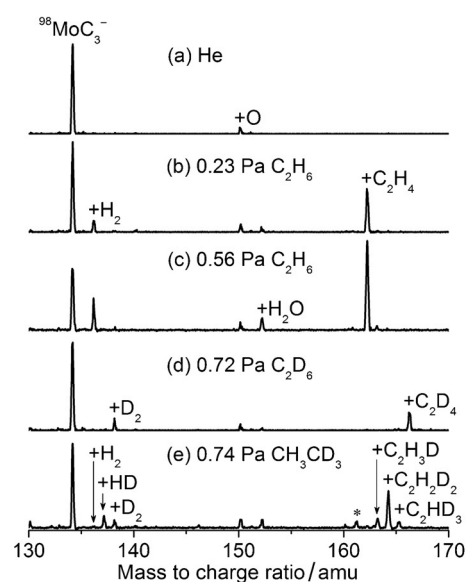
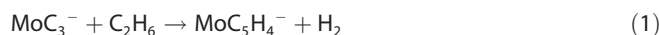


**Figure 1.** Cluster reactivity: Time-of-flight mass spectra for the reactions of mass-selected  $^{98}\text{MoC}_3^-$  with  $\text{C}_2\text{H}_6$  (b, c),  $\text{C}_2\text{D}_6$  (d), and  $\text{CH}_3\text{CD}_3$  (e). Panel a) shows the reference spectrum without ethane molecules in the reactor. The reactant gas pressures are shown and the reaction time was 6.4 ms. A weak peak marked by the asterisk in e) can be assigned to  $\text{MoC}_5\text{HD}^-$ , which is possibly due to the reaction of  $\text{MoC}_3^-$  with a trace amount of  $\text{CH}_2\text{CD}_2$  in the  $\text{CH}_3\text{CD}_3$  sample ( $\text{MoC}_3^- + \text{CH}_2\text{CD}_2 \rightarrow \text{MoC}_5\text{HD}^- + \text{HD}$ , see also Figure S1 of the Supporting Information).



The above reaction channels were confirmed in isotopic labeling experiments with  $\text{C}_2\text{D}_6$  (Figure 1 d). When partially deuterated compound  $\text{CH}_3\text{CD}_3$  was used as the reactant (Figure 1 e), products  $\text{MoC}_5\text{H}_2\text{D}_2^-$  (HD loss),  $\text{MoC}_5\text{HD}_3^-$  ( $\text{H}_2$  loss), and  $\text{MoC}_5\text{H}_3\text{D}^-$  ( $\text{D}_2$  loss) that correspond to reaction channel (1) were generated. The products corresponding to reaction channels (2) were also observable in the  $\text{CH}_3\text{CD}_3$  experiments. The relative intensities of the product ions with respect to the reactant ions in Figure 1 c–e indicate that  $\text{CH}_3\text{CD}_3$  is less reactive than  $\text{C}_2\text{H}_6$ , and  $\text{MoC}_3^- + \text{C}_2\text{D}_6$  is the least efficient reaction.

Figure 2 plots the signal variation of the reactant and product cluster ions in the  $\text{MoC}_3^- + \text{C}_2\text{H}_6$  reaction with respect to the  $\text{C}_2\text{H}_6$  pressure  $P$ . The relative intensity  $I_R$  of the reactant cluster  $\text{MoC}_3^-$  decreases from about 1.0 to 0.15 when the  $P$  value increases from 0 to about 1.0 Pa. The almost constant  $I_R$  value when  $P$  is greater than 1.0 Pa indicates that some of the experimentally generated  $\text{MoC}_3^-$  ions were inert toward  $\text{C}_2\text{H}_6$ . The  $I_R$  value could be well fitted by Equation (3)

$$I_R = x_{\text{inert}} + (1 - x_{\text{inert}}) \times \exp\left(-k \frac{P}{k_B T} t_R\right) \quad (3)$$

in which  $x_{\text{inert}}$  is the relative intensity of the unreactive component (isomer or electronic state) of  $\text{MoC}_3^-$ ,  $k_1$  the pseudo-first-order rate constant of the reactive component of  $\text{MoC}_3^-$ ,  $k_B$

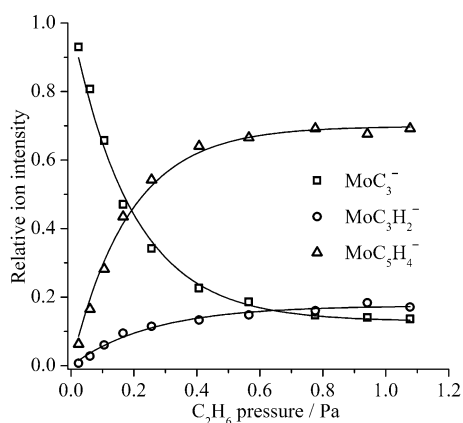


**Figure 2.** Reaction kinetics: Variation of ion intensities with respect to the C<sub>2</sub>H<sub>6</sub> pressure in the reaction of MoC<sub>3</sub><sup>-</sup> with C<sub>2</sub>H<sub>6</sub>. The solid lines were fitted to the experimental data points by using the equations derived with the approximation of the pseudo-first-order reaction mechanism for the reactive species [Eq. (3)].

the Boltzmann constant,  $t_R$  the reaction time [(6.4 ± 0.2) ms], and  $T$  the temperature of the reactant gas.<sup>[32]</sup> The gas temperature  $T$  is assumed to be close to the temperature of the wall of the reactor [(300 ± 5) K]. It is noteworthy that mass-selected atomic clusters in experiments may have different structural isomers that can have very different reactivity.

The  $x_{\text{inert}}$  and  $k_1$  parameters in Equation (3) were determined to be (13 ± 1)% and (2.23 ± 0.12) × 10<sup>-12</sup> cm<sup>3</sup> molecule<sup>-1</sup> s<sup>-1</sup>, respectively. The uncertainties of ± 1% and ± 0.12 × 10<sup>-12</sup> cm<sup>3</sup> molecule<sup>-1</sup> s<sup>-1</sup> correspond to one standard error in the least-squares fitting. Of the experimentally generated MoC<sub>3</sub><sup>-</sup> ions, (87 ± 1)% were reactive with C<sub>2</sub>H<sub>6</sub> and their relative intensity followed a single-exponential decay. In fitting the  $k_1$  parameter in Equation (3), the systematic deviations of  $t_R$  (± 3%),  $T$  (± 2%), and  $P$  (± 20%) were not considered. When these errors are taken into account, the uncertainty of the rate constant  $k_1(\text{MoC}_3^- + \text{C}_2\text{H}_6)$  is ± 0.47 × 10<sup>-12</sup> cm<sup>3</sup> molecule<sup>-1</sup> s<sup>-1</sup>, that is,  $k_1(\text{MoC}_3^- + \text{C}_2\text{H}_6)$  can be rewritten as (2.2 ± 0.5) × 10<sup>-12</sup> cm<sup>3</sup> molecule<sup>-1</sup> s<sup>-1</sup>. The branching ratios of reaction channels (1) and (2) by fitting the relative intensities of MoC<sub>3</sub>H<sub>4</sub><sup>-</sup> and MoC<sub>3</sub>H<sub>2</sub><sup>-</sup> are (81 ± 3)% and (19 ± 2)%, respectively (Figure 2). The kinetic isotopic effect (KIE)  $k_1(\text{MoC}_3^- + \text{C}_2\text{H}_6)/k_1(\text{MoC}_3^- + \text{CH}_3\text{CD}_3)$  is 1.9 ± 0.4 and  $k_1(\text{MoC}_3^- + \text{C}_2\text{H}_6)/k_1(\text{MoC}_3^- + \text{C}_2\text{D}_6)$  is 5.4 ± 0.6. The theoretical collision rate<sup>[33]</sup> between MoC<sub>3</sub><sup>-</sup> and C<sub>2</sub>H<sub>6</sub> is 9.6 × 10<sup>-10</sup> cm<sup>3</sup> molecule<sup>-1</sup> s<sup>-1</sup>, which means that the possibility of reaction on each collision is (0.23 ± 0.05)% for the reactive component of MoC<sub>3</sub><sup>-</sup>. The slow reaction is consistent with a large KIE [ $k_1(\text{MoC}_3^- + \text{C}_2\text{H}_6)/k_1(\text{MoC}_3^- + \text{C}_2\text{D}_6) = 5.4 ± 0.6$ ].

## Structure

Figure 3 shows the assignment of the ground-state structure of MoC<sub>3</sub><sup>-</sup> on the basis of the quantum chemical calculations and PEI spectroscopy. DFT calculations with TPSS functional<sup>[34]</sup> and 6-311 + G(d) basis sets<sup>[35]</sup> for C and H atoms and effective core potential (ECP)<sup>[36]</sup> combined with the polarized triple- $\zeta$  va-

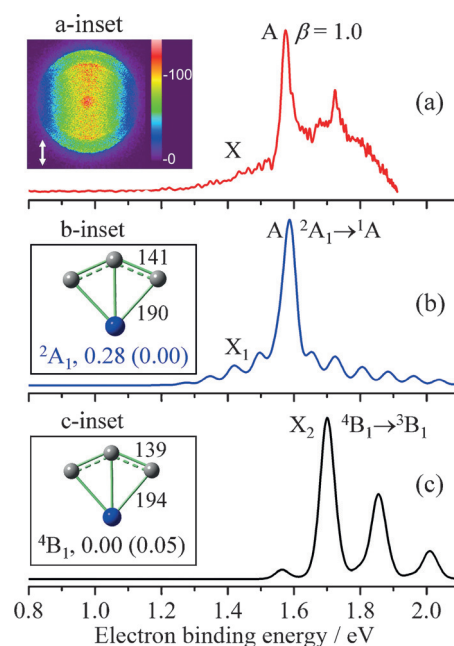


**Figure 3.** Structure characterization: Assignment of the MoC<sub>3</sub><sup>-</sup> structure on the basis of photoelectron spectrum by experiment (a) and FC simulations (b and c). The insets show the experimental photoelectron image (a inset) and the DFT calculated structures of MoC<sub>3</sub><sup>-</sup> (b inset and c inset). The image was recorded with a photon energy of 1.907 eV and more images can be found in Figure S2 of the Supporting Information. For the structures in the insets of b) and c), the bond lengths are in picometers and the relative energies at the TPSS (RCCSD(T)) levels are in electron volts. The sharp band marked as A in a) has an anisotropy parameter  $\beta$  of 1.0 ± 0.1. The electronic transitions X<sub>1</sub> (b), A (b), and X<sub>2</sub> (c) are <sup>2</sup>A<sub>1</sub> → <sup>3</sup>B<sub>1</sub>, <sup>2</sup>A<sub>1</sub> → <sup>1</sup>A, and <sup>4</sup>B<sub>1</sub> → <sup>3</sup>B<sub>1</sub>, respectively. In the FC simulations, the vibrational temperature was set to 700 K and each vibronic transition was convoluted with a resolution of 30 meV. Other parameters in the FC simulations were based solely on the DFT calculated results (band centers were neither shifted to match the experiment nor reordered according to the RCCSD(T) relative energies).

lence (Def2-TZVP) basis set<sup>[37]</sup> for Mo atom were performed to study the structure of MoC<sub>3</sub><sup>-</sup> and the reaction mechanism with C<sub>2</sub>H<sub>6</sub>. The DFT study determined two fanlike and one rodlike structures that are close in energy (0.28 eV). The rodlike structure (C<sub>3v</sub> <sup>4</sup>Σ<sup>-</sup>, Figure S5 in the Supporting Information) has a high adiabatic electron-detachment energy (ADE = 2.348 eV) according to the DFT calculations. The two fanlike structures (C<sub>2v</sub> <sup>2</sup>A<sub>1</sub> and <sup>4</sup>B<sub>1</sub>) have low ADEs of 1.415 and 1.698 eV, respectively. The experimental PEI spectra (Figure 3 a and Figure S2 of the Supporting Information) have a strong and sharp band marked as A at 1.575 ± 0.005 eV, which well matches the Franck–Condon (FC) simulation of the <sup>2</sup>A<sub>1</sub> (MoC<sub>3</sub><sup>-</sup>) → <sup>1</sup>A (MoC<sub>3</sub>) transition (calculated ADE = 1.582 eV). The <sup>2</sup>A<sub>1</sub> → <sup>3</sup>B<sub>1</sub> transition (calculated ADE = 1.415 eV) marked by X<sub>1</sub> in Figure 3 b has a broad FC profile, of which the left part matches the broad and weak feature marked by X (ADE = 1.4 ± 0.1 eV, see Figure S2 d for the details of deriving this value) in Figure 3 a. It can be concluded that the MoC<sub>3</sub><sup>-</sup> ions with the doublet state (<sup>2</sup>A<sub>1</sub>, Figure 3 b, inset) were populated in the experiment.

The strong signal of the A band (Figure 3 a and S2) suggests that the <sup>2</sup>A<sub>1</sub> state (Figure 3 b-inset) is the ground state of MoC<sub>3</sub><sup>-</sup>. However, the energy of the <sup>2</sup>A<sub>1</sub> state is higher than

that of the  $^4B_1$  state (Figure 3c, inset) by 0.28 eV at the DFT level of theory. With ab initio calculations at the level of restricted coupled-cluster method with single, double, and perturbative triple excitations method [RCCSD(T)], the energy ordering of these two states switches, which supports the experimental suggestion that the  $MoC_3^-$  cluster has a doublet rather than a quartet ground state. The  $^4B_1$  state is only 0.046 eV above the  $^2A_1$  state at the reliable RCCSD(T) level of theory. At 300 K, the Boltzmann population of the  $^4B_1$  state can be calculated to be 14.4%, which well matches ( $13 \pm 1$ )% of inert  $MoC_3^-$  ions in the reactivity study in which the temperature was around 300 K. The combination of experimental and computational results suggests that the low-spin  $^2A_1$  state corresponds to the 87% reactive component of  $MoC_3^-$ , while the high-spin  $^4B_1$  state corresponds to the 13% unreactive component of  $MoC_3^-$ . Since the  $^4B_1$  and  $^2A_1$  states are very close in energy, the  $X_2$  transition ( $^4B_1 \rightarrow ^3B_1$ ) shown in Figure 3c (by DFT) should overlap with the  $X_1$  transition ( $^2A_1 \rightarrow ^3B_1$ ) shown in Figure 3b. As a result, both the  $X_1$  and  $X_2$  transitions are responsible for the broad X band in the experiment (Supporting Information, Figure S2B), which explains the fact that the vibrational feature of the X band was not resolved.

### Reaction mechanism

The DFT calculated potential-energy profiles for reaction channels (1) and (2) are shown in Figure 4 for the doublet spin state. The reaction in the quartet spin state (Supporting Information, Figure S11) is subject to a high overall barrier of 0.60 eV, which further indicates that the  $^4B_1$  state (Figure 3c-

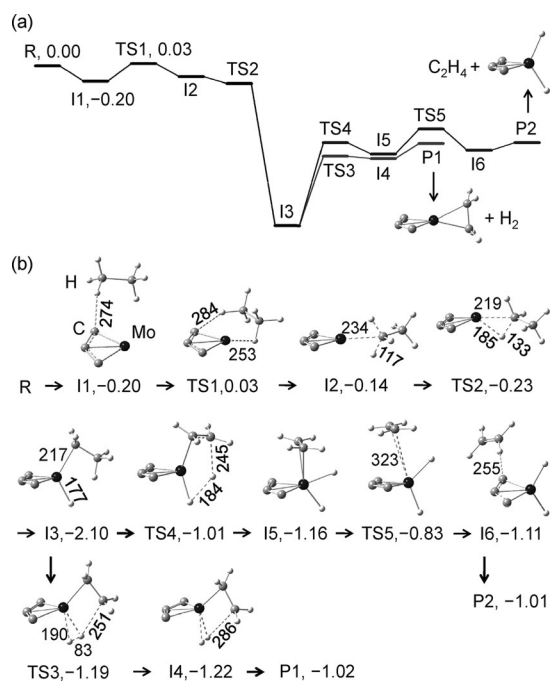


**Figure 4.** Reaction mechanism: DFT calculated potential-energy profiles and structures for the reaction of  $C_2H_6$  with  $MoC_3^-$  in the doublet spin state. The ZPE-corrected energies [eV] with respect to the separated reactants and some bond lengths [pm] are shown.

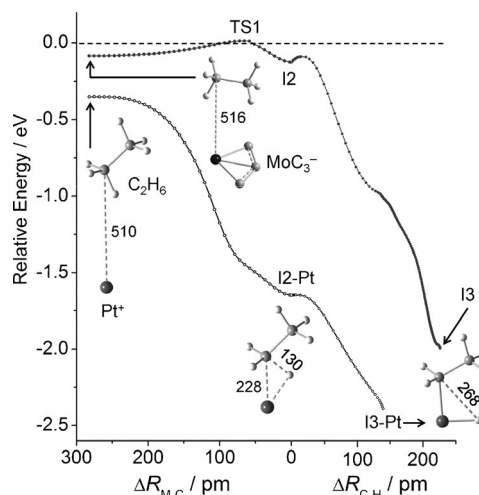


**Figure 5.** Shallow and deep entrance channels of ion-molecule reactions: DFT calculated relaxed potential-energy curves for approach of  $C_2H_6$  to M atom ( $M = Mo$  of  $MoC_3^-$  and  $M = Pt^+$ ) and the subsequent C–H bond cleavage.  $\Delta R_{M-C}$  (left) and  $\Delta R_{C-H}$  (right) are relative M–C and C–H distances with respect to those of the I2 (I2-Pt) complex, respectively. The optimized structures of  $C_2H_6Pt^+$  (I2-Pt) and  $C_2H_5PtH^+$  (I3-Pt) are shown. See Figure 4 for structures of TS1, I2, and I3.

inset) corresponds to the 13% unreactive component of  $MoC_3^-$  (Figure 2). The reaction of  $C_2H_6$  with the doublet  $MoC_3^-$  cluster (Figure 3b, inset) can take place with a negligible overall barrier (Figures 4 and 5) and the mechanism is described below.

When the  $MoC_3^-$  cluster interacts with  $C_2H_6$ , encounter complex I1 with a binding energy of 0.20 eV can be formed. After overcoming a small barrier [ $\Delta H_0(TS1) - \Delta H_0(I1) = 0.23$  eV], I1 is converted to I2, which is ready to form very stable complex through oxidative addition, insertion of the Mo atom into a C–H bond, and the concomitant formation of a Mo–H bond and a Mo– $C_2H_5$  bond. The oxidative addition releases enough energy (2.10 eV) to transform the reaction complex into products in the gas phase. This process ( $I2 \rightarrow TS2 \rightarrow I3$ ) is barrierless after zero-point vibrational energy (ZPE) corrections in the DFT calculations. The single-point energies of R ( $MoC_3^- + C_2H_6$ ), I1, TS1, I2, and TS2 in the DFT calculated structures were also calculated with the CCSD(T)/6-311+G(d)/Def2-TZVP method. In this case, the energies of I1, TS1, I2 and TS2 with respect to R are changed to  $-0.16$ ,  $-0.05$ ,  $-0.06$ , and  $-0.03$  eV (ZPE-corrected with DFT vibrational frequencies) from the DFT values of  $-0.20$ ,  $0.03$ ,  $-0.14$ , and  $-0.23$  eV, respectively.

To generate products  $MoC_3H_4^-$  and  $H_2$  (P1), the second hydrogen atom transfers ( $I3 \rightarrow TS3 \rightarrow I4$ ) from the  $C_2H_5$  moiety to make a chemical bond with the first hydrogen atom bonded with the Mo atom in I3. The H–H unit in I4 is loosely bonded with the Mo atom and the  $H_2$  elimination [reaction channel (1),  $\Delta H_0 = -1.02$  eV] is facile. To generate products  $MoC_3H_2^-$  and  $C_2H_4$  (P2), the second hydrogen atom transfers ( $I3 \rightarrow TS4 \rightarrow I5$ ) from the  $C_2H_5$  moiety to make a chemical bond with the Mo atom rather than the first hydrogen atom, which leads to the formation of two separate Mo–H bonds and a  $C_2H_4$  unit in I5. Then the ethene elimination [reaction channel (2),  $\Delta H_0 =$

–1.01 eV] proceeds via a transition state (I5→TS5→I6→P2) with a barrier of 0.33 eV. The energy of TS5 (–0.83 eV) is less negative than that of P1 (–1.02 eV), so reaction channel (1) is more favorable than channel (2), which is in agreement with the experimental observation (Figures 1 and 2).

Attempts to lose the H<sub>2</sub> molecule directly from I5 and I6 by shortening the H–H distance on the relaxed potential-energy surface scans were made (Supporting Information, Figure S9). These two paths proved to be less favorable than the I3→TS3→I4→P1 path. C–H activation by the carbon atom of MoC<sub>3</sub><sup>–</sup> (starting from I1, see Figure S10 of the Supporting Information) was also tested. Such a process is subject to overall positive reaction barrier of 0.78 eV. As a result, the Mo rather than the C atom is the active center for C–H activation by the MoC<sub>3</sub><sup>–</sup> anion.

The DFT results in Figure 4 can be used to qualitatively interpret the observed isotope scrambling in the CH<sub>3</sub>CD<sub>3</sub> experiment (Figure 1e): I4 and I5 can transform back into I3, which leads to scrambling of the hydrogen and deuterium atoms prior to the elimination of hydrogen and ethene molecules, respectively. Because I4 has C<sub>s</sub> symmetry, either of the two H atoms (H<sub>Mo</sub>) connected with the Mo atom in I4 can remake a C–H bond with one of the two C atoms in the back-formation of I3. Similarly, I5 also has C<sub>s</sub> symmetry, so one of the two H<sub>Mo</sub> atoms in I5 can remake a C–H bond with either of the two C atoms in the back-formation of I3. Note that if the hydrogen and deuterium atoms were completely scrambled prior to the hydrogen and ethene eliminations, the statistical distributions for the relative intensities of MoC<sub>5</sub>H<sub>3</sub>D<sup>–</sup>:MoC<sub>5</sub>H<sub>2</sub>D<sub>2</sub><sup>–</sup>:MoC<sub>5</sub>HD<sub>3</sub><sup>–</sup> [reaction (1)] and MoC<sub>3</sub>H<sub>2</sub><sup>–</sup>:MoC<sub>3</sub>HD<sup>–</sup>:MoC<sub>3</sub>D<sub>2</sub><sup>–</sup> [reaction (2)] would be 20:60:20 in both cases. The data obtained from our experiments (Figure 1e) are 20:67:13 for MoC<sub>5</sub>H<sub>3</sub>D<sup>–</sup>:MoC<sub>5</sub>H<sub>2</sub>D<sub>2</sub><sup>–</sup>:MoC<sub>5</sub>HD<sub>3</sub><sup>–</sup> and 12:59:29 for MoC<sub>3</sub>H<sub>2</sub><sup>–</sup>:MoC<sub>3</sub>HD<sup>–</sup>:MoC<sub>3</sub>D<sub>2</sub><sup>–</sup>, which roughly agree with the statistical distributions. The discrepancies can be caused by experimental errors or incomplete scrambling.

## Discussion

The quantum chemical calculations indicate that I1 is more stable than I2 [by 0.06 eV with DFT and 0.10 eV with CCSD(T)], so formation of I1 is preferred when C<sub>2</sub>H<sub>6</sub> approaches MoC<sub>3</sub><sup>–</sup>. There is a barrier [0.23 eV with DFT and 0.11 eV with CCSD(T)] for converting I1 to I2, which is generally consistent with the low reaction efficiency (0.23%) in the experiment. The reactive intermediate I2 may also be formed directly (R→I2, not involving I1). However, in such a case, the reactants must have the right orientation for approaching each other. To further understand the low efficiency of MoC<sub>3</sub><sup>–</sup> + C<sub>2</sub>H<sub>6</sub>, the minimum potential-energy curve to form I2 was carefully followed. The result is compared with that of the very efficient reaction (≈100%) Pt<sup>+</sup> + C<sub>2</sub>H<sub>6</sub>→PtC<sub>2</sub>H<sub>4</sub><sup>+</sup> + H<sub>2</sub><sup>[13c]</sup> in Figure 5. The difference between cationic and anionic reaction systems is obvious: the former has a much deeper entrance channel to form the encounter and insertion complexes than the latter. Moreover, Pt<sup>+</sup> is isotropic, whereas the active center (Mo) of MoC<sub>3</sub><sup>–</sup> is surrounded by the inert C<sub>3</sub> chain (Supporting Information, Fig-

ure S10). As a result, the anionic MoC<sub>3</sub><sup>–</sup> can be much less reactive than the cationic Pt<sup>+</sup> in the reaction with C<sub>2</sub>H<sub>6</sub>.

With respect to very fast gas-phase ion–molecule reactions ( $k_1 \approx 10^{-10} \text{ cm}^3 \text{ molecule}^{-1} \text{ s}^{-1}$ ), the reaction of MoC<sub>3</sub><sup>–</sup> + C<sub>2</sub>H<sub>6</sub> is very slow ( $k_1 \approx 2.2 \times 10^{-12} \text{ cm}^3 \text{ molecule}^{-1} \text{ s}^{-1}$ ). However, this gas-phase study identified that a properly engineered ETM center (see further discussion below) can activate the C–H bonds of a simple alkane molecule (C<sub>2</sub>H<sub>6</sub>) with rather low reaction barriers (0.11–0.23 eV, 2.5–5.3 kcal mol<sup>–1</sup>). Compared with condensed-phase reactions with typical activation barriers around 5–10 kcal mol<sup>–1</sup>,<sup>[3c,38]</sup> the C–H activation by the Mo center herein is relatively facile.

Many atomic cations (M<sup>+</sup>)<sup>[4–10]</sup> and ligated systems (ML<sup>+</sup>, L = H, CH<sub>3</sub>, etc.)<sup>[20f,h]</sup> can activate the C–H bonds of alkane molecules by oxidative addition under ambient conditions. These C–H oxidative additions usually take place in low-spin electronic states [e.g., Pt<sup>+</sup>, PdH<sup>+</sup>, and MCH<sub>3</sub><sup>+</sup> (M = Ru, Rh, Pt, Pd)] or proceed through a crossover from high-spin ground states with high reaction barriers to lower-spin excited states that have lower reaction barriers [e.g., M<sup>+</sup> (M = Ti, Nb, Ta, and Ir) and MCH<sub>3</sub><sup>+</sup> (M = Os and Ir)]. The importance of low-spin states in the C–H oxidative addition can be attributed to the availability of spin-paired electrons that facilitate s–d hybridization and formation of two covalent bonds in the insertion intermediate by using simple MO concepts developed previously for reactions of transition metal ions.<sup>[11]</sup> It turns out that this concept of the importance of low-spin states, developed from investigations of atomic cations, is valid for the MoC<sub>3</sub><sup>–</sup> cluster anion in this study.

The atomic species Mo<sup>+</sup>, Mo<sup>–</sup>, and Mo, which all have high-spin ground electronic states (<sup>6</sup>S, <sup>6</sup>S, and <sup>7</sup>S, respectively), have been experimentally found to be inert toward alkanes under thermal-collision conditions.<sup>[11c,27]</sup> Our DFT studies (see Supporting Information, Figure S12) confirmed that these high-spin ground states all have high C–H activation barriers, whereas their lower-spin excited states (<sup>4</sup>G/Mo<sup>+</sup>, <sup>4</sup>G/Mo<sup>–</sup>, and <sup>5</sup>S/Mo) have very small or negligible C–H activation barriers. Due to the high energy (> 1 eV) of reactive low-spin states, the spin-crossing points in the scenario of two-state reactivity<sup>[39]</sup> should be located high in energy, which prevents thermal C–H bond oxidative addition, as shown in Figure 6 (left). In contrast, the reactive low-spin state of MoC<sub>3</sub><sup>–</sup> is the ground state, and the unreactive high-spin state becomes the excited state. One can conclude that carbon can stabilize the reactive low-spin state of the early transition metal centers (Figure 6, right). Besides the MoC<sub>3</sub><sup>–</sup> anion in this study, two anionic carbonyl complexes, Mn(CO)<sub>3</sub><sup>–</sup> and Fe(CO)<sub>2</sub><sup>–</sup>, reported to be active for C–H oxidative addition in the late 1980s<sup>[40]</sup> were identified to have low-spin ground states as well.<sup>[41]</sup> In contrast, the naked metal ions Mn<sup>–</sup> and Fe<sup>–</sup> were not reported to be reactive toward simple alkanes. It is noteworthy that previous studies on cationic systems such as FeCO<sup>+</sup>, FeH<sub>2</sub>O<sup>+</sup>,<sup>[23a]</sup> Ti(CH<sub>4</sub>)<sub>2</sub><sup>+</sup>,<sup>[23b]</sup> and many others<sup>[12c,23c]</sup> also showed that the reactivity of metal centers could be altered by changing their ligation states. This study emphasizes that the relative energies of the low-spin states can be very important to interpret the ligand-dependent reactivity, particularly for the oxidative addition reactions.

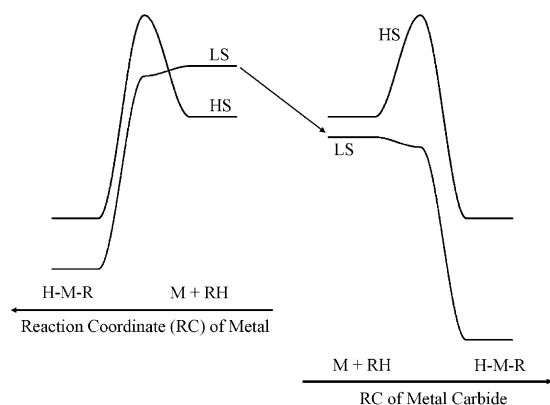


**Figure 6.** Carbon stabilizes reactive low-spin state: Simplified potential-energy profiles and energetics for the processes of C–H bond oxidative additions by naked metal atom (e.g., Mo, left) and metal carbide (e.g.,  $\text{MoC}_3^-$ , right) in low-spin (LS) and high spin (HS) states.

The bonding nature of metal carbides (MoC, NbC, etc.) has been subjected to extensive studies,<sup>[27]</sup> and it has been recognized that the electronic structures of metal carbides are more complex than those of the corresponding oxides and nitrides<sup>[27]</sup> because carbon has the smallest electronegativity among the elements C, N, and O. As a result, the paired electrons around the low-spin metal center of carbides can easily donate into the antibonding  $\sigma^*(\text{C-H})$  orbital of alkane molecules ( $\text{M}\uparrow\downarrow\rightarrow\sigma^*$ ), which weakens and finally cleaves the C–H bond through concomitant electron donation from the bonding  $\sigma(\text{C-H})$  orbital to the empty acceptor orbital on the metal ( $\text{M}^*\leftarrow\uparrow\downarrow\sigma$ ).<sup>[11]</sup> The  $\text{M}\uparrow\downarrow\rightarrow\sigma^*$  type electron donation can be primarily important for oxidative addition, in which the formal oxidation state of the metal center is increased by two units.<sup>[1c,2]</sup> The metal oxides and possibly nitrides can have less favorable  $\text{M}\uparrow\downarrow\rightarrow\sigma^*$ -type electron donation with respect to carbides, because the related metal centers surrounded with the O (or N) ligands should be less reductive. As a result, the ETM carbide clusters can reduce the C–H bonds through the metal centers. In sharp contrast, many ETM oxide clusters were identified to oxidize the C–H bonds by oxygen radicals through hydrogen-atom abstraction.<sup>[1f,24]</sup>

The C–H oxidative addition by  $\text{MoC}_3^-$  suggests that the interactions between carbon and ETM centers such as Mo can be just strong enough to stabilize low-spin electronic states that are reductive enough to activate the chemically inert C–H bond of alkanes. In heterogeneous catalysis, it was found that ETM oxides such as  $\text{MoO}_x$ -modified zeolite catalysts were not active enough for direct transformation of small alkanes into aromatics and hydrogen. Instead, the catalysts became active after an induction period in which the transition metal centers were carburized. The resulting carbide species such as MoC clusters were proposed to be active for the rate-determining C–H bond activation.<sup>[42]</sup> The mechanism by which carbon stabilizes the reactive low-spin state for oxidative addition revealed in this study provides a molecular-level basis to understand why carbides are important and how they can activate C–H bonds in related heterogeneous catalysis.

## Conclusion

The reaction of mass-selected molybdenum carbide cluster  $\text{MoC}_3^-$  with ethane in an ion-trap reactor produces ethene and hydrogen molecules under thermal-collision conditions. The  $\text{MoC}_3^-$  cluster has a fanlike geometry ( $C_{2v}$  point group) and low-spin ground electronic state ( $^2A_1$ ) on the basis of PEI spectroscopy and high-level quantum chemical calculations. The C–H activation of  $\text{C}_2\text{H}_6$  by  $\text{MoC}_3^-$  occurs by the mechanism of oxidative addition, which is more favorable in low-spin than in high-spin electronic states. The interaction between Mo and C atoms in  $\text{MoC}_3^-$  is strong enough to stabilize the low-spin state on the one hand, and on the other hand the interaction is weak enough so that the metal center can reduce the C–H bond in the oxidative addition. This study reveals that, to cleave the C–H bonds through oxidative addition, the unreactive ETM centers can be properly engineered to be reactive through carburization, which explains the importance of related metal carbides in heterogeneous catalysis.

## Experimental Section

### Experimental methods

A reflectron time-of-flight mass spectrometer (TOF-MS)<sup>[43]</sup> equipped with a laser ablation cluster source, a quadrupole mass filter (QMF),<sup>[44]</sup> and a linear ion-trap (LIT) reactor<sup>[32]</sup> was used to study the reactions of  $\text{MoC}_3^-$  with ethane. The  $\text{MoC}_3^-$  cluster ions were generated by laser vaporization of a rotating and translating molybdenum metal disk (compressed isotope-enriched  $^{98}\text{Mo}$  powder, 99.45%, Trace Science International) in the presence of 0.1%  $\text{CH}_4$  seeded in a He carrier gas with a backpressure of six standard atmospheres. The generated cluster ions were mass-selected by the QMF and then entered the LIT reactor, where they were thermalized by collisions with a pulse of He gas (8–10 Pa at ca. 300 K) for about 1.5 ms and then interacted with a pulse of ethane ( $\text{C}_2\text{H}_6$ ) for a period of time. The pulses delivering the gases into the LIT were short ( $\approx 300 \mu\text{s}$ ), whereas the decay times for the flow of the gases from the LIT to vacuum were long (5.1 and 16.4 ms for He and  $\text{C}_2\text{H}_6$ , respectively). Additional test spectra for interactions of  $\text{Fe}^\pm$  ions with small alkanes are shown in Figures S3 and S4 (Supporting Information). Fully and partially deuterated ethane  $\text{C}_2\text{D}_6$  (98% D, Cambridge Isotope Laboratories, Inc) and  $\text{CH}_3\text{CD}_3$  (98% D, Cambridge Isotope Laboratories, Inc) were also used to verify the assignments of the reaction channels and to study the isotope effect on the reaction. The cluster ions ejected from the LIT were detected by the TOF-MS. The details of running the instrument and the method to derive the rate constants of the reactions have been described in our previous works.<sup>[32,43,44]</sup>

Recently, our tandem TOF/TOF-MS for studying photoinduced reaction of mass-selected cluster ions<sup>[45]</sup> was modified by installing a home-designed PEI spectrometer. Briefly, the laser-ablated cluster anions passed through two identical reflectors with Z-shaped configuration in the primary TOF-MS, and then the ions of interest were selected by a mass gate to interact with a wavelength-tunable laser beam delivered from an optical parametric oscillator (Continuum, Horizon I) laser source. The velocities of the photodetached electrons were measured by the home-made PEI spectrometer, and the details are given in ref. [46]. The energy resolution is 3.0% at a kinetic energy of  $E_k = 1.0 \text{ eV}$ . Note that the cluster vibrational temperature in the PEI experiment could be higher than that in

the reactivity experiment, in which the cluster ions were subject to additional cooling in the LIT through collisions with the He gas. It has been demonstrated that the cluster ions in the LIT are thermalized ( $\approx 300$  K) before the reaction in previous studies on the reactivity of  $(V_2O_5)_nO^{-(32)}$  and  $PtAl_2O_4^{-(209)}$  clusters. It is noteworthy that the cluster ions formed in a narrow cluster generation channel were usually rotationally cold ( $T_{\text{vib}} \approx 50$  K) and vibrationally hot ( $T_{\text{vib}}$  up to 700 K).<sup>[47]</sup> It is difficult to determine the vibrational temperature of cluster ions in a spectroscopic study. As a result, we consider that the cluster vibrational temperature was close to 300 K in the reactivity study, while it could be in the range 300–700 K in the spectroscopic study.

### Computational details

The DFT calculations with Gaussian 09 program package<sup>[48]</sup> were carried out to investigate the structures of  $MoC_3^-$  and the reaction mechanism of  $MoC_3^- + C_2H_6$ . The reaction mechanism of  $Pt^+ + C_2H_6$  was also studied for comparison. The structures and energies of neutral  $MoC_3$  clusters were also studied to interpret the PEI experimental results. To find an appropriate functional, the bond-dissociation energies of Mo–C, H–C<sub>2</sub>H<sub>5</sub>, H–H, and C–C were computed with various functionals and compared with available experimental data (Supporting Information, Table S1). With the 6-311 + G (d)<sup>[35]</sup> basis set for C and H atoms and the effective core potential (ECP)<sup>[36]</sup> combined with the polarized triple- $\zeta$  valence (Def2-TZVP)<sup>[37]</sup> basis set for Mo, the TPSS functional<sup>[34]</sup> was the overall best functional and even better than the popular B3LYP functional, so the TPSS functional was adopted in the DFT calculations. The DFT calculated structures, energies, and vibrational frequencies (modes) were used to predict the FC profiles of the photoelectron spectra for the  $MoC_3^-$  cluster with doublet and quartet spin multiplicities. The FC simulations were performed with the ezSpectrum software suite,<sup>[49]</sup> and vibrational temperatures ranging from 300 to 700 K were tested. The ECP<sup>[36]</sup> combined with a D95V basis set<sup>[50]</sup> (denoted as SDD in Gaussian software) was used for the Pt atom in the reaction mechanism study of  $Pt^+ + C_2H_6$ .

To determine reliable relative energies of two lowest-lying electronic structures ( $^2A_1$  and  $^4B_1$  states) of the  $MoC_3^-$  cluster, single-point energy calculations with high-level quantum chemistry method of RCCSD(T)<sup>[51]</sup> were performed at the DFT optimized geometries. The Molpro program package<sup>[52]</sup> was used in the RCCSD(T) calculations in which the reference orbitals were from the complete active space self-consistent field (CASCF) calculations employing an active space composed of seven electrons distributed in seven orbitals covering the singly occupied molecular orbitals and high-lying valence orbitals. For Mo and C atoms, very large aug-cc-pwCVQZ-PP/aug-cc-pVQZ (abbreviated as AwQZ) and aug-cc-pwCV5Z-PP/aug-cc-pV5Z (abbreviated as Aw5Z) basis sets<sup>[53]</sup> were employed in RCCSD(T) calculations, and two-point complete basis set (CBS) limit extrapolation from AwQZ and Aw5Z data was conducted by using the inverse quartic equation  $E_{\text{Total},n} = E_{\text{Total,CBS}} + A/(n + 1/2)^4$  to alleviate the basis set incompleteness error.<sup>[54]</sup> In all these calculations, the Mo 4s4p core-valence correlation was included with the used basis set of Mo designed for this purpose. The scalar relativistic effect was taken into account by using the Stuttgart new relativistic energy-consistent small-core pseudopotential (PP) ECP28MDF in combination with the above basis set for the Mo atom.<sup>[53]</sup> To correct the error of this PP in treating scalar relativistic effects, we also did the RCCSD(T) calculations using the more accurate full electron second-order Douglas–Kroll–Hess (DKH) Hamiltonian<sup>[55]</sup> with the corresponding aug-cc-pwCVTZ-DK<sup>[53]</sup>/aug-cc-pVTZ-DK<sup>[56]</sup> basis sets on Mo and C atoms, and obtained the DKH correction by comparing the results

with those from calculations using PP and the aug-cc-pwCVTZ-PP/aug-cc-pVTZ basis set.<sup>[53]</sup> In all these calculations, for DKH correction of PP results, the Mo 4s4p core-valence correlation effect was considered. The final reported RCCSD(T) relative energy was obtained from the sum of the CBS data with the PP and DKH corrections.

The reaction-mechanism calculations by the DFT method involve geometry optimization of reaction intermediates and transition states (TSs). The TS optimizations were performed by using the Bery algorithm<sup>[57]</sup> from initial structures obtained through relaxed potential-energy surface scans with appropriate internal coordinates. Vibrational frequency calculations were performed to check that the reaction intermediates and transition states have zero and only one imaginary frequency, respectively. Intrinsic reaction coordinate<sup>[58]</sup> calculations were also performed to confirm that the transition structures actually connect two appropriate local minima in the reaction pathways. When appropriate, the ZPE-corrected energies were determined and given in this work.

### Acknowledgements

This work was supported by the Strategic Priority Research Program of the Chinese Academy of Sciences (XDA09030101), the National Natural Science Foundation of China (21325314, 21203208, 21290194, 21221002 and 21473215), and the Major Research Plan of China (2013CB834603). The support from the reviewers pointing out relevant literature references and making suggestions for improvements is acknowledged.

**Keywords:** carbides · C–H activation · density functional calculations · molybdenum · reaction mechanisms

- [1] a) J. A. Labinger, J. E. Bercaw, *Nature* **2002**, *417*, 507–514; b) B. A. Arndtson, R. G. Bergman, T. A. Mobley, T. H. Peterson, *Acc. Chem. Res.* **1995**, *28*, 154–162; c) D. Balcells, E. Clot, O. Eisenstein, *Chem. Rev.* **2010**, *110*, 749–823; d) J. Roithová, D. Schröder, *Chem. Rev.* **2010**, *110*, 1170–1211; e) H. Schwarz, *Angew. Chem. Int. Ed.* **2011**, *50*, 10096–10115; *Angew. Chem.* **2011**, *123*, 10276–10297; f) X.-L. Ding, X.-N. Wu, Y.-X. Zhao, S.-G. He, *Acc. Chem. Res.* **2012**, *45*, 382–390.
- [2] J. Halpern, *Acc. Chem. Res.* **1970**, *3*, 386–392.
- [3] a) A. Dedieu, *Chem. Rev.* **2000**, *100*, 543–600; b) M. Lersch, M. Tilset, *Chem. Rev.* **2005**, *105*, 2471–2526; c) R. Kang, W. Lai, J. Yao, S. Shaik, H. Chen, *J. Chem. Theory Comput.* **2012**, *8*, 3119–3127.
- [4] L. S. Sunderlin, P. B. Armentrout, *J. Am. Chem. Soc.* **1989**, *111*, 3845–3855.
- [5] R. Tonkyn, J. C. Weishaar, *J. Phys. Chem.* **1986**, *90*, 2305–2308.
- [6] N. Aristov, P. B. Armentrout, *J. Am. Chem. Soc.* **1986**, *108*, 1806–1819.
- [7] M. R. Sievers, P. B. Armentrout, *Organometallics* **2003**, *22*, 2599–2611.
- [8] M. R. Sievers, Y.-M. Chen, C. L. Haynes, P. B. Armentrout, *Int. J. Mass Spectrom.* **2000**, *195/196*, 149–170.
- [9] a) S. W. Buckner, T. J. MacMahon, G. D. Byrd, B. S. Freiser, *Inorg. Chem.* **1989**, *28*, 3511–3518; b) L. G. Parke, C. S. Hinton, P. B. Armentrout, *J. Phys. Chem. C* **2007**, *111*, 17773–17787.
- [10] P. B. Armentrout, S. Shin, R. Liyanage, *J. Phys. Chem. A* **2006**, *110*, 1242–1260.
- [11] a) X.-G. Zhang, R. Liyanage, P. B. Armentrout, *J. Am. Chem. Soc.* **2001**, *123*, 5563–5575; b) R. Georgiadis, P. B. Armentrout, *J. Phys. Chem.* **1988**, *92*, 7067–7074; c) R. Georgiadis, P. B. Armentrout, *Int. J. Mass Spectrom. Ion Processes* **1989**, *89*, 227–247; d) R. Z. Hinrichs, P. A. Willis, H. U. Stauffer, J. J. Schroden, H. F. Davis, *J. Chem. Phys.* **2000**, *112*, 4634–4643.
- [12] a) M. C. Michelini, I. Rivalta, E. Sicilia, *Theor. Chem. Acc.* **2008**, *120*, 395–403; b) L. L. Lv, Y. C. Wang, Z. Y. Geng, Y. B. Si, Q. Wang, H. W. Liu, *Organometallics* **2009**, *28*, 6160–6170; c) H. Schwarz, *Isr. J. Chem.* **2014**, *54*, 1413–1431.

- [13] a) P. A. M. van Koppen, M. T. Bowers, E. R. Fisher, P. B. Armentrout, *J. Am. Chem. Soc.* **1994**, *116*, 3780–3791; b) P. B. Armentrout, J. L. Beauchamp, *Acc. Chem. Res.* **1989**, *22*, 315–321; c) C. Adlhart, E. Uggerud, *Chem. Eur. J.* **2007**, *13*, 6883–6890; d) X.-N. Wu, X.-N. Li, X.-L. Ding, S.-G. He, *Angew. Chem. Int. Ed.* **2013**, *52*, 2444–2448; *Angew. Chem.* **2013**, *125*, 2504–2508.
- [14] a) D. Schröder, H. Schwarz, *Proc. Natl. Acad. Sci. USA* **2008**, *105*, 18114–18119; b) G. de Petris, A. Troiani, M. Rosi, G. Angelini, O. Ursini, *Chem. Eur. J.* **2009**, *15*, 4248–4252; c) S. M. Lang, T. M. Bernhardt, R. N. Barnett, U. Landman, *Angew. Chem. Int. Ed.* **2010**, *49*, 980–983; *Angew. Chem.* **2010**, *122*, 993–996; d) D. J. Harding, C. Kerpel, G. Meijer, A. Fielicke, *Angew. Chem. Int. Ed.* **2012**, *51*, 817–819; *Angew. Chem.* **2012**, *124*, 842–845; e) V. J. F. Lapoutre, B. Redlich, A. F. G. van der Meer, J. Oomens, J. M. Bakker, A. Sweeney, A. Mookherjee, P. B. Armentrout, *J. Phys. Chem. A* **2013**, *117*, 4115–4126.
- [15] a) D. K. Böhme, H. Schwarz, *Angew. Chem. Int. Ed.* **2005**, *44*, 2336–2354; *Angew. Chem.* **2005**, *117*, 2388–2406; b) Y. Gong, M. F. Zhou, L. Andrews, *Chem. Rev.* **2009**, *109*, 6765–6808; c) H. J. Zhai, L. S. Wang, *Chem. Phys. Lett.* **2010**, *500*, 185–195; d) Y.-X. Zhao, X.-N. Wu, J.-B. Ma, S.-G. He, X.-L. Ding, *Phys. Chem. Chem. Phys.* **2011**, *13*, 1925–1938; e) A. W. Castleman, Jr., *Catal. Lett.* **2011**, *141*, 1243–1253; f) S. M. Lang, T. M. Bernhardt, *Phys. Chem. Chem. Phys.* **2012**, *14*, 9255–9269; g) K. R. Asmis, *Phys. Chem. Chem. Phys.* **2012**, *14*, 9270–9281; h) S. Yin, E. R. Bernstein, *Int. J. Mass Spectrom.* **2012**, *321–322*, 49–65.
- [16] a) D. J. Trevor, D. M. Cox, A. Kaldor, *J. Am. Chem. Soc.* **1990**, *112*, 3742–3749; b) U. Achatz, C. Berg, S. Joos, B. S. Fox, M. K. Beyer, G. Niedner-Schatteburg, V. E. Bondybey, *Chem. Phys. Lett.* **2000**, *320*, 53–58; c) C. Adlhart, E. Uggerud, *Chem. Commun.* **2006**, 2581–2582.
- [17] S. M. Lang, A. Frank, T. M. Bernhardt, *J. Phys. Chem. C* **2013**, *117*, 9791–9800.
- [18] C. Adlhart, E. Uggerud, *J. Chem. Phys.* **2005**, *123*, 214709.
- [19] a) K. Koszinowski, D. Schröder, H. Schwarz, *ChemPhysChem* **2003**, *4*, 1233–1237; b) K. Koszinowski, D. Schröder, H. Schwarz, *J. Am. Chem. Soc.* **2003**, *125*, 3676–3677; c) K. Koszinowski, D. Schröder, H. Schwarz, *Angew. Chem. Int. Ed.* **2004**, *43*, 121–124; *Angew. Chem.* **2004**, *116*, 124–127.
- [20] a) R. H. Crabtree, M. F. Mellea, J. M. Mihelcic, J. M. Quirk, *J. Am. Chem. Soc.* **1982**, *104*, 107–113; b) B. L. Tjelta, P. B. Armentrout, *J. Am. Chem. Soc.* **1996**, *118*, 9652–9660; c) G. Albert, C. Berg, M. Beyer, U. Achatz, S. Joos, G. Niedner-Schatteburg, V. E. Bondybey, *Chem. Phys. Lett.* **1997**, *268*, 235–241; d) M. Schlangen, D. Schröder, H. Schwarz, *Chem. Eur. J.* **2007**, *13*, 6810–6816; e) M. Schlangen, H. Schwarz, *Angew. Chem. Int. Ed.* **2007**, *46*, 5614–5617; *Angew. Chem.* **2007**, *119*, 5711–5715; f) S. Liu, Z. Geng, Y. Wang, Y. Yan, *J. Phys. Chem. A* **2012**, *116*, 4560–4568; g) Y.-X. Zhao, Z.-Y. Li, Z. Yuan, X.-N. Li, S.-G. He, *Angew. Chem. Int. Ed.* **2014**, *53*, 9482–9486; h) M. Armélin, M. Schlangen, H. Schwarz, *Chem. Eur. J.* **2008**, *14*, 5229–5236.
- [21] a) C. Berg, T. Schindler, G. Niedner-Schatteburg, V. E. Bondybey, *J. Chem. Phys.* **1995**, *102*, 4870; b) Q.-F. Wu, W.-Y. Lu, S.-H. Yang, *J. Chem. Phys.* **1998**, *109*, 8935.
- [22] S.-G. He, Y. Xie, F. Dong, E. R. Bernstein, *J. Chem. Phys.* **2006**, *125*, 164306.
- [23] a) P. B. Armentrout, B. L. Tjelta, *Organometallics* **1997**, *16*, 5372–5374; b) P. A. M. van Koppen, P. R. Kemper, J. E. Bushnell, M. T. Bowers, *J. Am. Chem. Soc.* **1995**, *117*, 2098–2099; c) P. B. Armentrout, *Acc. Chem. Res.* **1995**, *28*, 430–436.
- [24] N. Dietl, M. Schlangen, H. Schwarz, *Angew. Chem. Int. Ed.* **2012**, *51*, 5544–5555; *Angew. Chem.* **2012**, *124*, 5638–5650.
- [25] a) L. Wang, L. Tao, M. Xie, G. Xu, J. Huang, Y. Xu, *Catal. Lett.* **1993**, *21*, 35; b) D. Ma, Y. Shu, M. Cheng, Y. Xu, X. Bao, *J. Catal.* **2000**, *194*, 105; c) J. Gao, Y. Zheng, J.-M. Jehng, Y. Tang, I. E. Wachs, S. G. Podkolzin, *Science* **2015**, *348*, 686.
- [26] a) F. Solymosi, R. Németh, *Catal. Lett.* **1999**, *62*, 197; b) F. Solymosi, R. Németh, L. Óvári, L. Egri, *J. Catal.* **2000**, *195*, 316.
- [27] a) B. C. Guo, S. Wei, J. Purnell, S. Buzza, A. W. Castleman, *Science* **1992**, *256*, 515–516; b) B. C. Guo, K. P. Kerns, A. W. Castleman, *Science* **1992**, *255*, 1411–1413; c) D. S. Bethune, R. D. Johnson, J. R. Salem, M. S. Devries, C. S. Yannoni, *Nature* **1993**, *366*, 123–128; d) X. Li, L. S. Wang, *J. Chem. Phys.* **1999**, *111*, 8389–8395; e) H. Shinohara, *Rep. Prog. Phys.* **2000**, *63*, 843; f) M. M. Rohmer, M. Bénard, J. M. Poblet, *Chem. Rev.* **2000**, *100*, 495–542; g) S.-B. Cheng, A. W. Castleman, *J. Phys. Chem. A* **2014**, *118*, 6935–6939; h) I. León, Z. Yang, L.-S. Wang, *J. Chem. Phys.* **2014**, *140*, 084303; i) Z. Luo, H. Huang, Z. Zhang, Y.-C. Chang, C. Y. Ng, *J. Chem. Phys.* **2014**, *141*, 024304.
- [28] a) C. J. Cassidy, S. W. Mcelvany, *J. Am. Chem. Soc.* **1990**, *112*, 4788–4797; b) H. T. Deng, K. P. Kerns, R. C. Bell, A. W. Castleman, *Int. J. Mass Spectrom.* **1997**, *167*, 615–625; c) K. Miyajima, N. Fukushima, F. Mafune, *J. Phys. Chem. A* **2008**, *112*, 5774–5776; d) Z.-Y. Li, Z. Yuan, Y.-X. Zhao, S.-G. He, *Chem. Eur. J.* **2014**, *20*, 4163–4169.
- [29] a) R. R. Squires, *Chem. Rev.* **1987**, *87*, 623–646; b) P. B. Armentrout, *J. Phys. Chem. A* **2006**, *110*, 8327–8338.
- [30] J.-H. Meng, X.-J. Deng, Z.-Y. Li, S.-G. He, W.-J. Zheng, *Chem. Eur. J.* **2014**, *20*, 5580–5583.
- [31] a) D. M. Neumark, *J. Phys. Chem. A* **2008**, *112*, 13287; b) I. León, Z. Yang, H.-T. Liu, L.-S. Wang, *Rev. Sci. Instrum.* **2014**, *85*, 083106.
- [32] Z. Yuan, Z.-Y. Li, Z.-X. Zhou, Q.-Y. Liu, Y.-X. Zhao, S.-G. He, *J. Phys. Chem. C* **2014**, *118*, 14967–14976.
- [33] a) G. Gioumousis, D. P. Stevenson, *J. Chem. Phys.* **1958**, *29*, 294–299; b) G. Kummerlöwe, M. K. Beyer, *Int. J. Mass Spectrom.* **2005**, *244*, 84–90.
- [34] J. Tao, J. P. Perdew, V. N. Staroverov, G. E. Scuseria, *Phys. Rev. Lett.* **2003**, *91*, 146401.
- [35] R. Krishnan, J. S. Binkley, R. Seeger, J. A. Pople, *J. Chem. Phys.* **1980**, *72*, 650.
- [36] D. Andrae, U. Häußermann, M. Dolg, H. Stoll, H. Preuß, *Theor. Chim. Acta* **1990**, *77*, 123–141.
- [37] F. Weigend, R. Ahlrichs, *Phys. Chem. Chem. Phys.* **2005**, *7*, 3297–3305.
- [38] a) B. Zhou, H. Chen, C. Wang, *J. Am. Chem. Soc.* **2013**, *135*, 1264–1267; b) X. Yang, *ACS Catal.* **2013**, *3*, 2684–2688; c) Y. T. Lee, Y. K. Kang, Y. K. Chung, *J. Org. Chem.* **2009**, *74*, 7922–7934.
- [39] D. Schröder, S. Shaik, H. Schwarz, *Acc. Chem. Res.* **2000**, *33*, 139–145.
- [40] a) R. N. McDonald, M. T. Jones, *J. Am. Chem. Soc.* **1986**, *108*, 8097–8098; b) R. N. McDonald, D. J. Reed, A. K. Chowdhury, *Organometallics* **1989**, *8*, 1122–1124.
- [41] a) L. S. Sunderlin, D. Wang, R. R. Squires, *J. Am. Chem. Soc.* **1993**, *115*, 12060–12070; b) L. Andrews, M. Zhou, X. Wang, C. W. Bauschlicher, *J. Phys. Chem. A* **2000**, *104*, 8887–8897; c) G. Wang, C. Chi, J. Cui, X. Xing, M. Zhou, *J. Phys. Chem. A* **2012**, *116*, 2484–2489.
- [42] a) J. Shu, A. Adnot, B. P. A. Grandjean, *Ind. Eng. Chem. Res.* **1999**, *38*, 3860–3867; b) H. Zheng, D. Ma, X. Bao, J. Z. Hu, J. H. Kwak, Y. Wang, C. H. F. Peden, *J. Am. Chem. Soc.* **2008**, *130*, 3722–3723; c) D. Zhou, S. Zuo, S. Xing, *J. Phys. Chem. C* **2012**, *116*, 4060–4070.
- [43] X.-N. Wu, B. Xu, J.-H. Meng, S.-G. He, *Int. J. Mass Spectrom.* **2012**, *310*, 57–64.
- [44] Z. Yuan, Y.-X. Zhao, X.-N. Li, S.-G. He, *Int. J. Mass Spectrom.* **2013**, *354–355*, 105–112.
- [45] B. Xu, J.-H. Meng, S.-G. He, *J. Phys. Chem. C* **2014**, *118*, 18488–18495.
- [46] Q.-Y. Liu, L. Hu, Z.-Y. Li, C.-G. Ning, J.-B. Ma, H. Chen, S.-G. He, *J. Chem. Phys.* **2015**, *142*, 164301.
- [47] Y. Matsuda, E. R. Bernstein, *J. Phys. Chem. A* **2005**, *109*, 3803–3811.
- [48] Gaussian 09, Revision A.1, M. J. Frisch, G. W. Trucks, H. B. Schlegel, G. E. Scuseria, M. A. Robb, J. R. Cheeseman, G. Scalmani, V. Barone, B. Menucci, G. A. Petersson, H. Nakatsuji, M. Caricato, X. Li, H. P. Hratchian, A. F. Izmaylov, J. Bloino, G. Zheng, J. L. Sonnenberg, M. Hada, M. Ehara, K. Toyota, R. Fukuda, J. Hasegawa, M. Ishida, T. Nakajima, Y. Honda, O. Kitao, H. Nakai, T. Vreven, J. A. Montgomery, J. E. Peralta, F. Ogliaro, M. Bearpark, J. J. Heyd, E. Brothers, K. N. Kudin, V. N. Staroverov, R. Kobayashi, J. Normand, K. Raghavachari, A. Rendell, J. C. Burant, S. S. Iyengar, J. Tomasi, M. Cossi, N. Rega, J. M. Millam, M. Klene, J. E. Knox, J. B. Cross, V. Bakken, C. Adamo, J. Jaramillo, R. Gomperts, R. E. Stratmann, O. Yazyev, A. J. Austin, R. Cammi, C. Pomelli, J. W. Ochterski, R. L. Martin, K. Morokuma, V. G. Zakrzewski, G. A. Voth, P. Salvador, J. J. Dannenberg, S. Dapprich, A. D. Daniels, O. Farkas, J. B. Foresman, J. V. Ortiz, J. Cioslowski, D. J. Fox, Gaussian, Inc., Wallingford CT, **2009**.
- [49] V. A. Mozhayskiy, A. I. Krylov, ezSpectrum 3.0, see <http://iopshell.usc.edu/downloads>.
- [50] M. Dolg, H. Stoll, H. Preuss, *J. Chem. Phys.* **1989**, *90*, 1730–1734.
- [51] a) K. Raghavachari, G. W. Trucks, J. A. Pople, M. Head-Gordon, *Chem. Phys. Lett.* **1989**, *157*, 479–483; b) J. D. Watts, J. Gauss, R. J. Bartlett, *J. Chem. Phys.* **1993**, *98*, 8718–8733; c) P. J. Knowles, C. Hampel, H. J. Werner, *J. Chem. Phys.* **1993**, *99*, 5219–5227.
- [52] H. J. Werner, P. J. Knowles, R. Lindh, F. R. Manby, M. Schütz, P. Celani, T. Korona, A. Mitrushenkov, G. Rauhut, T. B. Adler, R. D. Amos, A. Bern-

- hardsson, A. Berning, D. L. Cooper, M. J. O. Deegan, A. J. Dobbyn, F. Eckert, E. Goll, C. Hampel, G. Hetzer, T. Hrenar, G. Knizia, C. Köppl, Y. Liu, A. W. Lloyd, R. A. Mata, A. J. May, S. J. McNicholas, W. Meyer, M. E. Mura, A. Nicklass, P. Palmieri, K. Pflüger, R. Pitzer, M. Reiher, U. Schumann, H. Stoll, A. J. Stone, R. Tarroni, T. Thorsteinsson, M. Wang, A. Wolf, MOLPRO, version 2010.1, a package of ab initio programs. See <http://www.molpro.net>.
- [53] a) T. H. Dunning, *J. Chem. Phys.* **1989**, *90*, 1007–1023; b) K. A. Peterson, D. Figgen, M. Dolg, H. Stoll, *J. Chem. Phys.* **2007**, *126*, 124101.
- [54] a) J. M. L. Martin, *Chem. Phys. Lett.* **1996**, *259*, 669–678; b) D. Feller, K. A. Peterson, J. G. Hill, *J. Chem. Phys.* **2011**, *135*, 044102.
- [55] a) M. Reiher, A. Wolf, *J. Chem. Phys.* **2004**, *121*, 2037–2047; b) M. Reiher, A. Wolf, *J. Chem. Phys.* **2004**, *121*, 10945–10956.
- [56] W. A. de Jong, R. J. Harrison, D. A. Dixon, *J. Chem. Phys.* **2001**, *114*, 48–53.
- [57] H. B. Schlegel, *J. Comput. Chem.* **1982**, *3*, 214–218.
- [58] C. Gonzalez, H. B. Schlegel, *J. Chem. Phys.* **1989**, *90*, 2154–2161.

---

Received: August 4, 2015

Published online on October 22, 2015